



Applying GPR-FGRA hybrid algorithm for prediction and optimization of eco-friendly magnetorheological finishing Ti–6Al–4V alloy

Dung Hoang Tien¹ · Trinh Nguyen Duy¹ · Pham Thi Thieu Thoa¹

Received: 7 May 2022 / Accepted: 16 July 2022 / Published online: 14 August 2022
© The Author(s), under exclusive licence to Springer-Verlag France SAS, part of Springer Nature 2022

Abstract

To produce the mirror finish of the Ti–6Al–4V alloy workpieces, a newly developed polishing tool based on magnetic field assistance. This work has developed an environmentally friendly model of magnetic finishing with a carrier fluid natural origin combined with carbonyl and abrasive iron particles; and a new GPR-FGRA hybrid algorithm to predict, optimize and identify critical factors affecting material removal rate and surface quality. The best surface quality with the optimization method increased by 37.5% ($R_a = 0.025 \mu\text{m}$) when choosing the optimized cutting parameter with the GPR-FGRA hybrid algorithm compared with the Taguchi experimental analysis ($R_a = 0.040 \mu\text{m}$). The analysis results by the GPR-FGRA algorithm show that the prediction surface quality accuracy was more significant than 99.63%, and the working distances (K) had the most remarkable influence on the polishing effect, while the result of workpiece speed was the least important. This study provides excellent reference values for predicting, optimizing and identifying the main factors affecting surface quality and material removal rate in a polishing model for complex, expensive materials from low-cost and environmentally friendly materials.

Keywords Magnetorheological finishing · Ti–6Al–4V alloy · GPR-FGRA · Polishing · Surface roughness · Eco-friendly

1 Introduction

Ti–6Al–4V alloy has a melting point and excellent wear resistance and is widely used in industry [1, 2]. With the excellent properties inherent to Ti–6Al–4V alloys, such as elasticity, high adhesion ability, and superior corrosion resistance, Ti–6Al–4V alloy classing as one of the most challenging materials to machine [3–5]. Therefore, to meet the increasingly stringent requirements from the industries, the finishing process for Ti–6Al–4V alloy machining workpiece super-gloss poses a significant challenge for manufacturers and technicians. Traditional surface finishing techniques such as grinding have improved machining surface quality. However, the poor grinding property of Ti–6Al–4V alloy leads to fast wheel wear that increases costs. Besides, the grinding surface quality and efficiency are lower than other materials [6–8]. Therefore, to produce a super-glossy surface with very high precision, a non-traditional surface finishing process is

required. The polishing under the support of magnetic fields is emerging as the advanced finishing method for high-gloss and precision finishes.

Magnetorheological finishing (MRF) forms by mixing a carbonyl iron particle (CIP) and abrasive particle (AP) with a carrier liquid to create a flexible polishing tool [9, 10]. MRF polishing tool works like Newton liquid when without a magnetic field. When there is a magnetic field, MRF immediately changes viscosity to a semisolid state (non-Newton liquid). When there is an impact magnetic field, this process is formed the chain structure by the interaction between magnetic particles that arrange themselves according to the magnetic field lines. The chain structure exhibits deformation resistance when removing residual materials under different machining modes. The rheological characteristics and the yield strength of the developed MR fluid affects by the externally applied magnetic field [10, 11]. The CIP in the MRF creates an interlinked chain along the direction of the magnetic field, resulting in a semisolid abrasive tool to process hard surfaces [12]. Barman et al. [13] studied the effect of magnetorheological polishing fluid compositions on the surface finish of Ti-alloy. Ultra-fine surface roughness was acquired when using different types of rheological fluids and observed that utilising a raster path provided the best

✉ Trinh Nguyen Duy
nguyenduytrinh@hau.edu.vn

¹ Faculty of Mechanical Engineering, Hanoi University of Industry, 298 Cau Dien, Bac Tu Liem District, Ha Noi, Vietnam

surface finish and surface topography at a rotational tool speed of 1200 rpm, a working gap of 1 mm, and a finishing time of 6.30 h. Nagdeve et al. [14] developed a rotational-magnetorheological abrasive flow finishing process-based unique tool for nano-finishing the knee joint's femoral component and surface finish in the 78–89 nm was attained by considering the effect of various input process parameters. The roughness parameters have obtained the values in the range of nanometers and rendered better surface topography [15]. Magnetorheological (MR) fluids are used by mixing with abrasive particles as finishing media for surface finishing. Singh et al. developed a ball-end tool formed by MR polishing medium for nano-finishing of 3D surfaces, the surface roughness of the ferromagnetic workpieces was reduced from 414.1 nm to 70 nm in 100 min [16]. Parameswari et al. [13] explored the critical quality performance of the MRF process in achieving nanolevel finish on Ti–6Al–4V flat discs. The initial surface roughness parameter significantly affects the finishing. MRF is primarily used to finish optics in nanometer surface roughness without sub-surface damage [17]. MRF has been successfully used to complete a wide variety of materials to sub-nanometer surface roughness values from initial sub-micrometre surface roughness values.

The MRFs apply successfully to finish Ti alloy and various materials to sub-nanometer surface roughness values from initial sub-micrometre surface roughness values. However, these studies have not addressed the issue of environmental protection from carrier fluids derived from vegetable oils. In the MRF polishing processes, the biodegradability of carrier fluids in the MRF is less critical than during their use. It depends mainly on the carrier medium used in the liquid synthesis. Silicon oil, mineral oil, hydrocarbon oil, and deionized water use commonly carrier fluids. In which deionized water can biodegrade in the environment, but with low viscosity, APs and CIPs deposited quickly. Furthermore, the deionized water components in MRF polishing are often in an acidic or alkaline environment to increase the magnetism in the carrier fluid. Consequently, CIP particles corrode and oxidize over time, reducing liquid structures' magnetic and yield stress. Deionized water-based carrier fluids cannot maintain the high temperature obtained during machining. Therefore, necessary to implement unique methods to overcome these problems, such as adding additives to reduce sedimentation and enhance thermal stability, creating a coating for magnetic particles to avoid corrosion and improve the carrier liquid, etc., which will increase the cost of the synthetic fluid. From the above problems and combined with biodegradation, it is essential to find an environmentally friendly alternative carrier liquid and overcome the disadvantages of deionized water.

The Gaussian Process Regression (GPR) algorithm is a powerful and flexible tool capable of providing confidence

intervals for prediction and optimization [18]. Zhang et al. [19] gave a multi-responsive GPR model and showed superiority through surface reaction. Besides the advantages of the GPR model, there are also limitations, such as not fully describing the influencing factors from technological parameters and not identifying the most and most minor influential factors that affect the survey subjects. Also, optimization problem solving is preeminent but based on the objective and explicit boundary functions. It has not established sufficient empirical relationships and has not solved the identification problem thoroughly. The authors integrated fuzzy grey relationship analysis (FGRA) into the GPR model to overcome these shortcomings. Based on the fuzzy system approach, the importance and uncertainty factors in the considering weights by different criteria in the FGRA model [20, 21]. The factors affecting the survey subjects are effectively measured and statistical by FGRA. This method is very suitable for solving problems of incomplete information, little input data or lots of data but sporadic, uncertain and inconsistent. The FGRA method is used in many fields, in which many researchers have optimized the processing parameters. The grey relation level indicates the similarity between the comparison and reference sequences [22, 23].

From the above characteristics, the authors have introduced a new polishing method with MRF containing inexpensive CIPs and APs. The carrier liquid is a safe and eco-friendly cutting oil solution combined with a new hybrid algorithm for a super precise mirror polishing surface. In this work, after describing the principles and operating principles of the MRF model, setting up the proposed Gaussian Process Regression and Fuzzy grey relationship analysis (GPR-FGRA) hybrid algorithm. Experimental processes on the Ti–6Al–4V workpiece aim to analyze the effects of technical parameters on MRR and surface quality. The optimal parameters in the MRF polishing process aim to increase surface quality and save machining time. The proposed method provides excellent reference values to further improve the surface quality and MRR capability.

2 Methodology and experimental design

The created MRF polishing process by a suspension of micrometre-sized (about 20–50 mm) magnetized particles in the carrier liquid, with a magnetization particle volume percentage of 30–40%. The ability to change behaviour under the impact of the magnetic field is a crucial feature of MRF. When no magnetic field exists, the liquid behaves like a regular liquid with properties close to the carrier liquid. MRF acts as a semi-solid substance when there is a magnetic field impact [24]. The CIPs in MRF with deionized water in nature is easily oxidized and dehydrated. Depending on working conditions, iron particles will be oxidized quickly

Fig. 1 Morphology of MRFs with different carrying fluids by the time

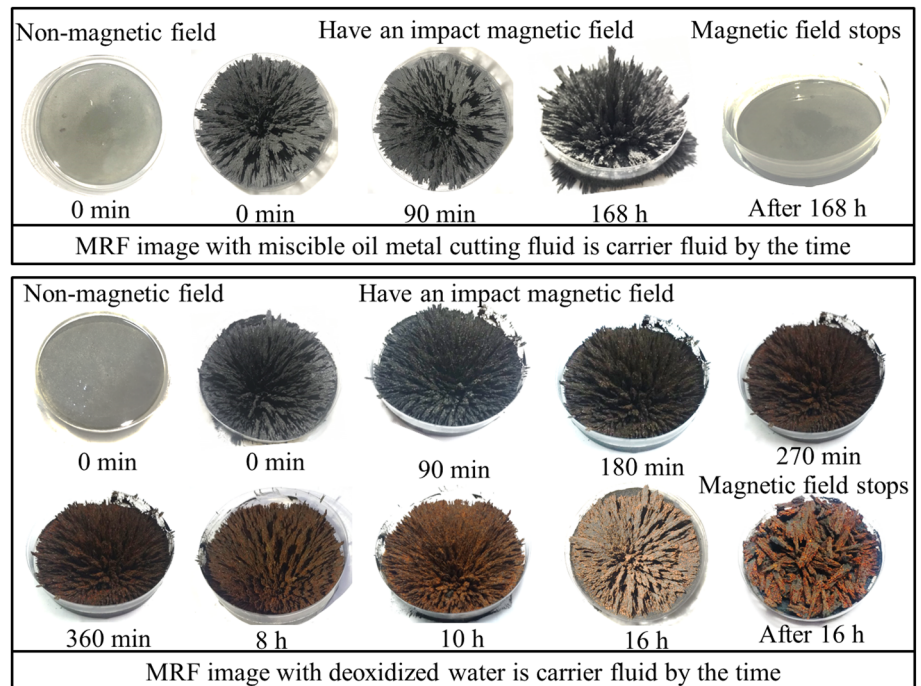
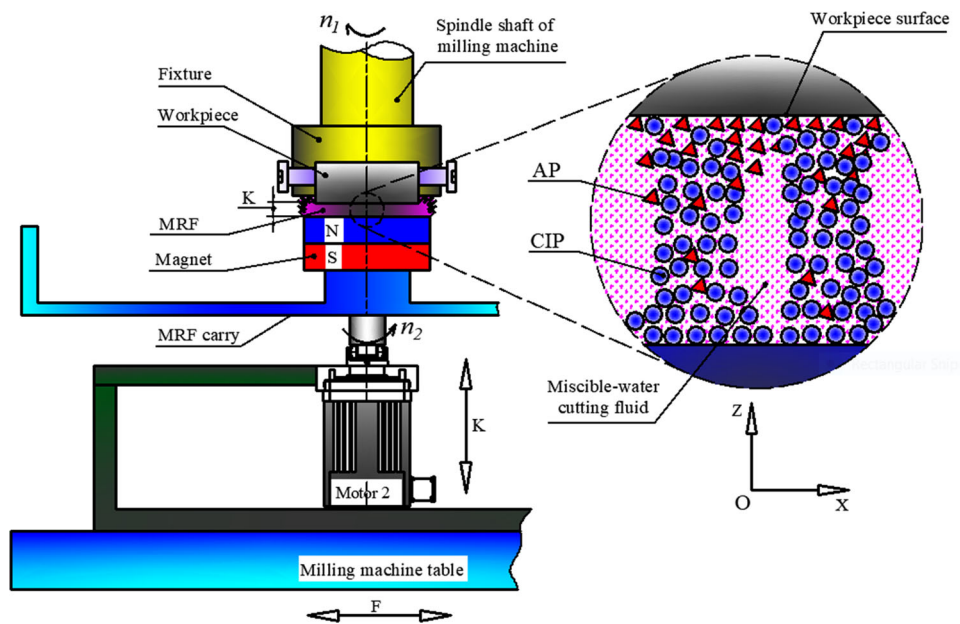


Fig. 2 MRF polishing principle



or slowly with time, humidity and temperature. Magnetic particle oxidation directly affects MRF behaviour in practical applications because iron oxides have inferior magnetic properties compared to pure iron. MRF with CIP oxidized showed a 20% decrease in magnetic effect. Figure 1 indicates that the MRF with the proposed carrier solution has a high viscosity, excellent oxidation resistance, and almost no oxidation over time. When not affected by an active magnetic field, the MRF returns to its original state. It can see that the proposed liquid is not only environmentally friendly but

also overcomes the phenomenon of ferromagnetic particles in the MRF oxidized and dehydrated, reducing viscosity and polishing ability over time as previous work encountered.

Figure 2 shows the principle of polishing operation by MRF. The workpiece is attached to the milling machine spindle via a fixture and has a rotational speed of n_1 . The permanent magnet placed on the MFC carries material SUS 304, and rotation is transmitted by motor 2. The direction of rotation of the MRF carrier is opposite to that of the milling

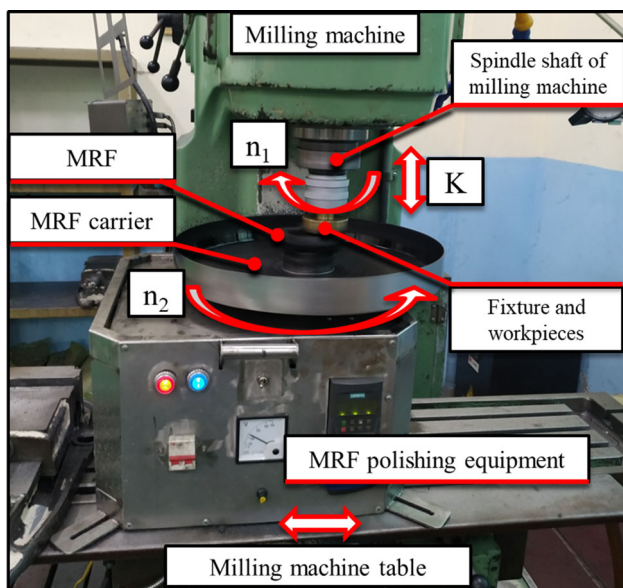


Fig. 3 MRF experimental equipment

machine spindle. The working distance (K) changes by moving the milling machine table up or down. The polishing device is located on the milling machine table to create horizontal tooling movement when polishing. At this point, the polishing settings by MRF have been forming. The experimental equipment setup and determination of MRR and surface roughness before and after polishing as shown in Figs. 3 and 4.

When setting a working distance (K), the CIP move in chains along the magnetic induction lines and non-magnetic AP are affected by gravity and exerted by a pulling force. Most of the non-magnetic APs in the MRF will move onto the workpiece surface as these force components act. The rotation of the workpiece and the MRF carrier will generate cutting forces of APs on the workpiece surface during machining. The AP receive rotation rate n_2 from the

MRF carrier. The micrometre size APs will remove minimal machining residual due to friction between the APs and the workpiece surface. The MRF should be set up directly above the permanent magnet to increase the polishing force between the APs and the workpiece. The magnetic system of permanent magnets making of N50 type Nd-Fe-B material. The experiment equipment in the MRF polishing system consists of a milling machine, a permanent magnetic, a fixture, a surface roughness meter, an electronic scale and an MRF carrier.

Table 1 describes the material specifications of the components used in the MRF polishing of Ti–6Al–4V alloy workpieces. Table 2 shows the composition of the different MRFs used in the polishing processes. The miscible oil with vegetable ester-based is cutting fluid manufactured by Vasco Jemtech Advanced Fluid Management, the CIPs with particle size 20–30 μm from manufacturer Henan Yuhuang Powder Metallurgy Plant. The AP (Al_2O_3) have a particle size of 30 μm and is manufacturing by Dengfeng Hongsheng Abrasives.

Polishing with individual abrasive particles has many effects that need to consider. The main influences on the MRF polishing process are the material composition and behaviour and the ability to achieve high gloss and precision for machined surface quality. The material removal factors need investigating to optimize MRF polishing elements. Preston was the first to adopt a mathematical model for material removal during liquid abrasive machining called Preston's law [25].

$$R = p \times v \times k \quad (1)$$

where p is the initial pressure at the contact zone, v is the relative velocity between the workpiece and the fluid in the polishing zone, and k is the Preston coefficient. The polishing method by MRF depends on the fluid properties, workpiece geometry, material properties and so on, as described in Eq. (1). However, to describe the general physical properties

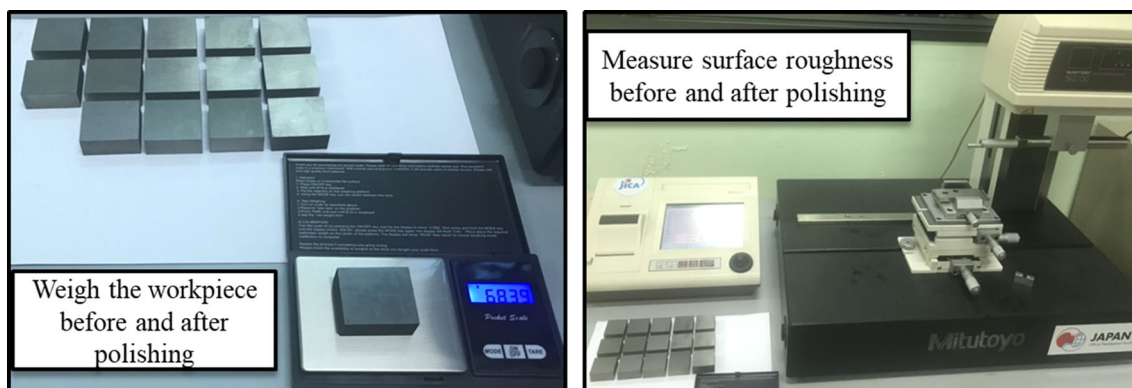


Fig. 4 Determination of MRR and surface roughness before and after polishing

Table 1 Material parameters used in Ti–6Al–4V alloy polishing

Mumerical order	Description	Material	Size	Relative magnetic permeability	Magnitude (A/m)
1	Permanent magnets	Nd-Fe-B	100 × 80 × 30 mm	1.09966	– 890,000
2	MRF carrier	SUS 304		1	
3	Polishing tool	MRF		5	
4	Workpiece	Ti–6Al–4V	32 × 32 × 20 mm	1	

Table 2 MRF components

Mumerical order	Description	Particles size (µm)	Percentage of components in the MRF (%)	Magnetic permeability (N/A ²)	Magnetic sensitivity	Specific weight (kg/cm ³)
1	CIP	20–30	40	$\mu = 5.03 \times 10^{-4}$	$\chi_m = 10^3$	$\rho_C = 7.8 \times 10^{-3}$
2	AP	30	12		$\chi'_m = 10^3$	$\rho_A = 3.965 \times 10^{-3}$
3	Miscible oil cutting fluid		45			$\rho_A = 0.9187 \times 10^{-3}$
4	α-cellulose		3			

of MRF processes, it is necessary to use an extended equation. The Equation of. The equation of Zhang et al. [26] includes process parameters that depend on the physical properties of the MR fluid through a complex relationship, as shown by Eq. (2) for the pressure distribution.

$$p = \left[\frac{-2\mu \times u \times x \times \eta_0}{h^2} + 3\phi\mu_0\mu_f \times \frac{\mu_p - \mu_f}{\mu_p + 2\mu_f} \times \int_0^H H dH \right] \tag{2}$$

where η_0 is the kinematic viscosity of the fluid and u is the velocity of the fluid, $\eta_0 = \nu \times \rho$ shows that the initial viscosity of the liquid η_0 can be calculated from the liquid density ρ and the kinematic viscosity ν . The parameters μ is related to the magnetic field, μ_0 is the magnetic permeability of the vacuum, μ_f is the magnetic permeability of the liquid, and μ_p is the magnetic permeability of the magnetic particles in

the fluid given by ϕ and the magnetic strength field provided by H .

The distance between the workpiece surface and the carrier for the liquid at each position is given by the actual distance K . The actual distance h depends on the depth of cut a_e and the MRF height h_0 , as shown in Eq. (3).

$$K = h_0 - a_e \tag{3}$$

Experimental to analyze the consistency between material removal and the listed MRF parameters. Factors investigated during MRF polishing, including MRF carrier speed, workpiece speed, the working distance (K) and feed rate, are shown in Tables 3 and 5.

Nowadays, machining process studies strive to exploit environmental safety features while preserving machining properties such as good abrasion resistance, low volatility, maintaining viscosity and ability to work at high temperatures, non-toxic, easy to biodegradable, etc. Studies of [27]

Table 3 Parameter level of MRF polishing technology according to the Taguchi method

Level	Workpiece speed (n_w) (rpm)	Working distances (K) (mm)	MRF carrier speed (n_{MRF}) (rpm)	Feed rate (F) (mm/min)
1	530	1	25	250
2	720	1,25	30	500
3	980	1,5	35	750
4	1330	1,75	40	900

Table 4 Components by weight of miscible water cutting fluid-based vegetable oils

Mumerical order	Material	Percentage (%)	Mumerical order	Material	Percentage (%)
1	Vegetable oils	5–20	6	Anti-rust agents	0–3
2	Synthetic esters of vegetable oils	15–35	7	Extreme pressure agents	0–3
3	Waters	5–15	8	Aseptic	0–2
4	Emulsifying agents	2–12	9	Defoamer	0–2
5	Dispersing agents	0–2	10	Alkaline reserve	15–30

Table 5 Experiment parameters for polishing Ti–6Al–4V alloy by MRF

Experiments order	Factor and level				MRR (mg/min)	Average surface roughness value R_{a_m} (μm)
	Workpiece speed (n_w)	MRF carrier speed (n_{MRF})	Feed rate (F)	Working distance (K)		
1	1	1	1	1	13.33	0.041
2	1	2	2	2	11.66	0.059
3	1	3	3	3	10	0.089
4	1	4	4	4	7.67	0.098
5	2	1	2	3	14.15	0.044
6	2	2	1	4	12.83	0.050
7	2	3	4	1	10.50	0.057
8	2	4	3	2	9.21	0.079
9	3	1	3	4	15.30	0.067
10	3	2	4	3	13.26	0.080
11	3	3	1	2	10.83	0.081
12	3	4	2	1	9.33	0.091
13	4	1	4	2	15.92	0.040
14	4	2	3	1	14.02	0.059
15	4	3	2	4	11.17	0.062
16	4	4	1	3	9.60	0.071

for a vegetable oil-based water-soluble cutting liquid have solved the above requirements. On that basis, the per cent components by weight of the cutaneous fluid, as described in Table 4.

Taguchi experiment method is applied in polishing by MRF to save many experiments and time from getting the optimal target group [28]. According to this approach, the impact levels of the survey factors are established based on the orthogonal array. In this work, the MRF polishing experiments for Ti–6Al–4V titanium alloy were set up according to the Taguchi experimental design, as shown in Table 5. Together with the constraints for cutting parameters are described in Table 6. Before polishing, the workpieces were

Table 6 Constraints on cutting parameters

Mumerical order	Constraint factor	Constraint range
1	Working distance (mm)	$0.3 < K < 5$
2	Feed rate (mm/min)	$2 < f < 3500$
3	Spindle speed (rpm)	$100 < n < 2100$
4	Carrier speed (rpm)	$0 < n < 60$

ground on a single crystal diamond grinding wheel, giving a surface roughness of about $R_a = 0.49 \mu\text{m}$.

Before polishing, the workpiece cleaning with ethanol and acetone. The MRR (mg/min) was determined by a high-resolution electronic balance (0.1 mg) as expressed by the equation:

$$MRR = \frac{\Delta m \times 10^3}{T} \quad (4)$$

where Δm : the mass difference before and after polishing (g), T : polishing time (min).

The surface quality obtained after polishing is determined by the average value of three measurements at different locations using the Mitutoyo SJ-400 roughness meter. Surface morphology of the workpiece after polishing observed by electron microscopy.

3 Modeling prediction and optimization of MRF polishing process Al–6Ti–4V alloy

3.1 Set up GPR-FGRA hybrid algorithm for predicting and optimizing the polishing process Ti–6Al–4V alloy

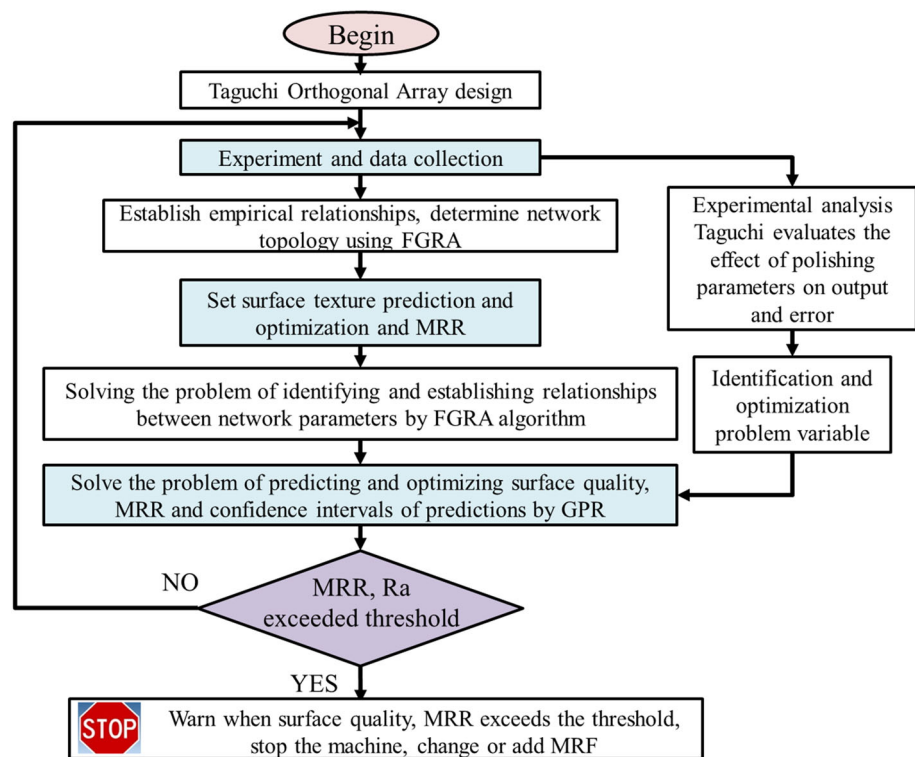
Prediction and optimization for the polishing process Al–6Ti–4V alloy belong to the experiment problem. With the approach from Taguchi's empirical analysis, the GPR-FGRA hybrid algorithm applying provides predictive parameters

and optimizes the ability of MRR and surface quality when polishing by MRF, as depicted in Fig. 5.

The GPR-FGRA hybrid algorithm includes the steps described as follows:

- Step 1. Set up an experimental model according to Taguchi analysis. The experiment processes are analyzed based on survey factors and levels.
- Step 2. Conduct experiment steps and data collection. Ti–6Al–4V alloy polishing steps constructing in the L16 orthogonal array.
- Step 3A. Give empirical relationships and random values by algorithm GPR and FGRA.
- Step 3B. Experimental analysis by the Taguchi method affecting the polishing process of Ti–6Al–4V alloy. The experiment analysis results decide to repeat the experiment or proceed with the previously established investigations.
- Step 4A. Set up the prediction model and optimize surface quality and MRR when polishing Ti–6Al–4V alloy. The analysis results give the optimal parameters from specific polishing conditions.
- Step 4B. Given the smallest and largest impact factors in polishing surface quality and MRR. The experimental results give the problem of surface quality optimization and MRR. This process makes it cost-effective to polish the Ti–6Al–4V alloy.

Fig. 5 The structure of the GPR-FGRA hybrid algorithm



- Step 5. Problem solve of identifying and establishing the relationship between network parameters by the FGRA algorithm.
- Step 6. Predict the surface quality, MRR and polishing interval confidence using MRF according to GPR.
- Step 7. Optimization and prediction parameters compared with surface texture parameters and critical threshold MRR. Predicted parameters more significant or smaller than the prediction threshold will go to step 8 and back to step 2, respectively.
- Step 8. Stop the polishing device when the predicted parameter equals or exceeds the critical value. When the survey parameters approach, the limit value will give warnings.

GPR-FGRA hybrid algorithm approach combined with Taguchi experimental parameters when polishing Ti–6Al–4V alloy, the disadvantages of the traditional polishing method are reduced and add new stages. To overcome the

weaknesses of conventional polishing methods, such as giving experimental relationships when using the GPR-FGRA hybrid algorithm to increase the ability to predict surface quality, MRR and that reliability of prediction and optimization. Applying GPR-FGRA hybrid algorithm to predict and optimize the polishing model with target functions set from the GPR algorithm increases the proposed model’s flexibility, predictability, and optimization. Adding a new stage to the polishing model: The experimental polishing model has determined the influence of technology modes on surface quality, thereby validating the reliability of the experiment implementation method and data collection.

3.2 Convergence and optimization solution of GPR-FGRA

Hybrid algorithm GPR-FGRA proposed when applied to multimodal functions (F10–F12) and non-modal (F1–F9) [29], as described in Table 7.

Table 7 Nonmodal Benchmark functions and polynomial equation with MRR and Ra

Func	Description	Range	Global minimum
<i>Nonmodal benchmark functions</i>			
F-1	$\sum_{i=1}^n (x_i^2)$	$x \in [-100, 100]$	0
F-2	$\sum_{i=1}^B [100 \times (x_i^2 - x_{i+1})^2 + (1 - x_i)^2]$	$x \in [-10, 10]$	0
F-3	$y \times [\sin(4x)] + 1.1x \times [\sin(2y)]$	$x, y \in [-10, 10]$	-19.8625
F-4	$\sum_{i=1}^n [x_i^2 - 10 \times \cos(2\pi x_i)] + 10 \times n$	$x \in [-5.12, 5.12]$	0
F-5	$-20 \times e^{\left[-0.2\sqrt{\frac{1}{30} \sum_{i=1}^B x_i^2}\right]} - e^{\left[-0.2\sqrt{\frac{1}{30} \sum_{i=1}^B \cos(2\pi x_i)}\right]}$	$x \in [-30, 30]$	$8.8818e^{-16}$
F-6	$\sum_{i=1}^n \cos(x_i) \times [x_i^2 + x_i]$	$x \in [-10, 10]$	-100.22365
F-7	$\sum_{i=1}^n (x_i - 10 \cdot \cos[\sqrt{ x_i }])$	$x \in [-10, 10]$	-10
F-8	$\frac{\sin^2\left[\sqrt{\frac{x_1^2+x_2^2}{0.001 \times (x_1^2+x_2^2)+1}}\right]-0.5}{0.001 \times (x_1^2+x_2^2)+1} + \frac{1}{2}$	$x_1, x_2 \in [-10, 10]$	0
F-9	$1 - \prod_{i=1}^n \cos\left[\frac{x_i}{\sqrt{i}}\right] + \sum_{i=1}^n \frac{(x_i^2)}{4000}$	$x \in [-10, 10]$	0.29289
<i>Polynomial equation with MRR and surface quality when polishing Ti–6Al–4V alloy</i>			
F-10	$MRR = -7.60409 + 0.0133498 \times n_w - 9.86072 \times K + 1.76568 \times n_{MRF} - 0.0158805 \times F - 0.0000149638 \times n_w^2 + 0.00319454 \times n_w \times K + 0.000372297 \times n_w \times n_{MRF} - 0.00000274302 \times n_w \times F + 1.96309 \times n_{MRF}^2 - 0.456901 \times K \times n_{MRF} + 0.0175629 \times K \times F - 0.0186909 \times n_{MRF}^2 - 0.000326395 \times n_{MRF} \times F + 0.00000460377 \times F^2$		
F-11	$Ra = -0.840419 + 0.000481304 \times n_w + 0.391957 \times K + 0.036819 \times n_{MRF} - 0.000553489 \times F - 1.73741E-7 \times n_w^2 - 0.0000710729 \times n_w \times K - 0.00000273123 \times n_w \times n_{MRF} - 2.50774E-8 \times n_w \times F - 0.020918 \times n_{MRF}^2 - 0.456901 \times K \times n_{MRF} - 0.0109927 \times K \times F - 0.000336342 \times n_{MRF}^2 - 0.00000371069 \times n_{MRF} \times F + 1.54043E-7 \times F^2$		

The following formula determines the stop criteria of the algorithm:

$$f_{End}(GPR - FGRA[M]) - Glo \leq S.CA \quad (5)$$

where $f_{End}(GPR - FGRA[M])$ is the value corresponding to the solution, which is best obtained at the last iteration of the algorithm, and $S.CA$ is the stop criterion of the algorithm. This criterion will converge with tolerances 10^{-6} and 10^{-3} corresponding to non-modal and multimodal functions, respectively.

The standard deviation with the obtained results is shown as follows:

$$S.AD = \left(\frac{1}{n} \sum_{i=1}^n [x_i - \bar{x}]^2 \right)^{\frac{1}{2}} \quad (6)$$

where x_i is the solution result vector run by the algorithm and \bar{x} is the average value of solutions determined by the following formula:

$$\bar{x} = \frac{1}{n} \sum_{i=1}^n x_i \quad (7)$$

The results include the best, mean and worst values and standard deviation (S.AD) after 50 times of independent implementation with the proposed GPR-FGRA and then compared with GSA, ABC, BBO, PSO and TLBO algorithms as shown in Table 8.

Table 8 shows the proposed GPR-FGRA for the best performance. The GPR-FGRA clearly shows its superiority and effectiveness in finding a search solution and has a lower standard deviation than other algorithms. Furthermore, in the case of the worst solution, GPR-FGRA has shown its excellence amongst the different algorithms by benchmark functions. Hence, with non-modal objective functions, in terms of solutions and quality, GPR-FGRA shows superiority to other well-known algorithms. However, this superiority does not manifest in all benchmark functions following the convergence capability. The convergence feature of GPR-FGRA was investigated and compared with the optimal algorithms of GSA, BBO, PSO, ABC and PLBO. Figure 6 shows the excellent convergence rate of GPR-FGRA compared to previously mentioned algorithms.

When applying algorithms for polynomial functions with MRR and surface roughness (F-10, F-11) based on time, the average value (mean value of all algorithm runs) and the optimal average value (average number of peaks found above 50 runs with $S.CA = 1000$), as shown in Table 9. The results show that the possibility of polynomial functions with MRR and surface roughness is not as high as non-modal functions. The complexity of the benchmark functions from F-10 and

F-11 increases, thereby reducing the quality of solutions. The average optimization value (AO) corresponding to the function F-10 is 19.1. However, the AO value with the function F-11 achieved by GPR-FGRA is 0.025. The results show that the quality obtained by GPR-FGRA is superior to the algorithms mentioned in most cases. Therefore, the proposed hybrid algorithm GPR-FGRA is highly applicable for identification and optimization when polishing Ti-6Al-4V alloy.

4 Results and discussion

Predicting and optimizing MRR and surface quality is determined through the experimental process. Aim to confirm the accuracy of the prediction model. The experiments were repeated three times with different machining conditions. Used the initial two datasets for training procedures and the third set of tests to predict the MRR and surface quality.

The prediction diagram of MRR and surface quality according to different cutting modes is shown in Figs. 7 and 8. The results of MRR prediction, as described in Fig. 7, show that the prediction error is less than 4.24% (the prediction accuracy is more than 95.76%). The accuracy of the GPR-FGRA hybrid algorithm for surface roughness prediction is higher than 99.63%, as illustrated in Fig. 8. Thus, the predicted parameters from the GRP-FGRA algorithm close with measurements and provide the confidence interval of the proposed prediction is 98%, as shown in Figs. 7 and 8.

Figure 9 shows the SEM surface morphology before and after finishing with MRF proposed for some experiments polishing Ti-6Al-4V. Figure 9 shows the results of surface roughness. Experimental results show that corresponding to different polishing technology modes will have different MRR and surface quality. It can see that the polishing experiments all yielded a significantly improved surface quality compared to the original grinding surface. Figure 10 depicted the surface roughness (Ra) before and after finishing the experiments. The workpiece surfaces Ti-6Al-4V alloy initial ($Ra \approx 0.35 \mu\text{m}$) significantly improve with $Ra < 0.1 \mu\text{m}$ under different test conditions.

Experimental results show that experiment number 13 gives the best surface quality corresponding to polishing distance $K = 1 \text{ mm}$, workpiece speed 1330 rpm, MRF carrier speed 40 rpm and feed rate $F = 500 \text{ mm/min}$. A mirror surface $Ra = 0.040 \mu\text{m}$ is produced by these polishing parameters. With experiment 4, polishing distance $K = 1.75 \text{ mm}$, spindle speed 530 rpm, MRF carrier speed 40 rpm and feed rate $F = 900 \text{ mm/min}$, for maximum roughness but still shown the mirror surface $Ra = 0.098 \mu\text{m}$ after this polishing process. Experimental procedures showed different surface qualities produced by other technological parameters when polishing Ti-6Al-4V alloy. However, the polishing surfaces are all

Table 8 Optimal solution obtained on non-modal functions

Func	Characteristics	Optimization algorithms					
		GSA	BBO	PSO	ABC	TLBO	GPR-FGRA
F-1	Best	5.8265	4.4548	4.15×10^{-14}	0.0369	3.25×10^{-6}	0
	Medium	15.2532	17.3493	8.98×10^{-12}	0.4283	9.35×10^{-5}	0
	Worst	24.0363	52.3655	1.84×10^{-10}	1.4497	0.0011	0
	S.AD	4.0362	10.7951	2.69×10^{-11}	0.3498	1.81×10^{-4}	0
F-2	Best	0.0085	0.0305	3.14×10^{-16}	5.62×10^{-7}	6.82×10^{-5}	0
	Medium	0.348	1.1483	375×10^{-9}	0.0016	2.43×10^{-2}	0
	Worst	1.1295	5.5835	4.96×10^{-8}	0.0175	0.1656	0
	S.AD	0.2915	1.3058	1.04×10^{-8}	0.0036	0.0325	0
F-3	Best	-19.7734	-19.7338	-19.8625	-19.8624	-19.8625	-19.8625
	Medium	-18.5456	-18.3465	-17.0658	-19.8624	-19.8623	-19.8625
	Worst	-17.4263	-16.8586	-11.6432	-19.8622	-19.8584	-19.8626
	S.AD	0.5189	0.6635	1.9550	4.46×10^{-10}	5.72×10^{-4}	1.68×10^{-6}
F-4	Best	1.0313	0.0112	0	1.98×10^{-6}	0	0
	Medium	4.2553	0.6125	1.3720	0.3132	2.53×10^{-13}	0
	Worst	7.7232	1.7141	4.9718	1.6948	5.02×10^{-12}	0
	S.AD	1.5538	0.4819	1.3154	0.4332	8.79×10^{-13}	0
F-5	Best	4.8954	1.4845	5.33×10^{-8}	0.1133	0.0028	8.88×10^{-16}
	Medium	6.1778	2.8952	0.1716	0.4016	0.0452	8.88×10^{-16}
	Worst	7.3043	4.7716	1.6463	1.3312	0.9551	8.88×10^{-16}
	S.AD	0.5293	0.5990	0.4348	0.2695	0.1333	0
F-6	Best	-200.4396	-200.4472	-200.4476	-200.4476	-200.4473	-200.4474
	Medium	-199.0867	-199.9673	-150.7991	-200.0686	-200.4472	-200.4475
	Worst	-193.2685	-198.2015	-89.8413	-181.5917	-200.4475	-200.4470
	S.AD	1.3388	0.5862	42.3978	2.6665	1.56×10^{-12}	1.07×10^{-4}
F-7	Best	-45.7485	-87.5372	-76.7760	-76.2008	-80.2418	-100
	Medium	-39.1212	-77.646	-65.9420	-65.3394	-73.1428	-100
	Worst	-32.0332	-71.1917	-61.2958	-59.7663	-67.8235	-100
	S.AD	3.5163	3.8413	4.2107	3.4835	2.8902	0
F-8	Best	3.61×10^{-5}	2.80×10^{-5}	0	0	1.23×10^{-4}	0
	Medium	0.0074	0.0403	0.0162	9.46×10^{-10}	0.0165	0
	Worst	0.0266	0.0446	0.0448	4.71×10^{-8}	0.0403	0
	S.AD	0.0065	0.0124	0.0218	6.66×10^{-9}	0.0105	0
F-9	Best	0.3206	0.0167	0	4.38×10^{-4}	6.35×10^{-5}	0
	Medium	0.5895	0.0578	0.0398	0.1269	0.0336	0
	Worst	0.7472	0.1128	0.1228	0.4573	0.0458	0
	S.AD	0.1002	0.0223	0.0314	0.1068	0.0165	0

mirror-like, thereby demonstrating the effectiveness of the proposed polishing method.

The polishing experiments with MRF performed by Parameswari et al. [30] apply to the polishing process of Ti-6Al-4V alloy from grinding surfaces with an average surface roughness $R_a = 0.415 \text{ mm}$. After polishing by Parameswari et al. [30], the workpiece obtained the best surface quality with $R_a = 94 \text{ nm}$ ($0.094 \text{ }\mu\text{m}$). As described in Figs. 9 and 10, our experimental results show that the surface quality from the proposed method is significantly improved compared to before polishing. The experiment processes corresponding to different polishing technology modes will have different MRR and surface quality. However, it can see that

the surface quality obtained from our experiments is significantly improved compared to the method proposed by Parameswari et al. [30]. Our study resulted in the best surface quality corresponding to $R_a = 40 \text{ nm}$, and the surface quality improved by 57.44% compared with the proposed method by Parameswari et al. [30].

Figures 11 and 12 show a 3D image visually describing the relationship between input parameters and survey parameters R_a and MRR given by the GPR-FGRA. Figure 11a, d illustrate the relationship between working distance (K) and workpiece speed, MRF carrier speed. The slight MRR values correspond to a high working distance (K), workpiece speed, and low MRF carrier speed. The MRR value increases with decreasing working distance (K) and increasing workpiece

Fig. 6 Ability to converge with different algorithms

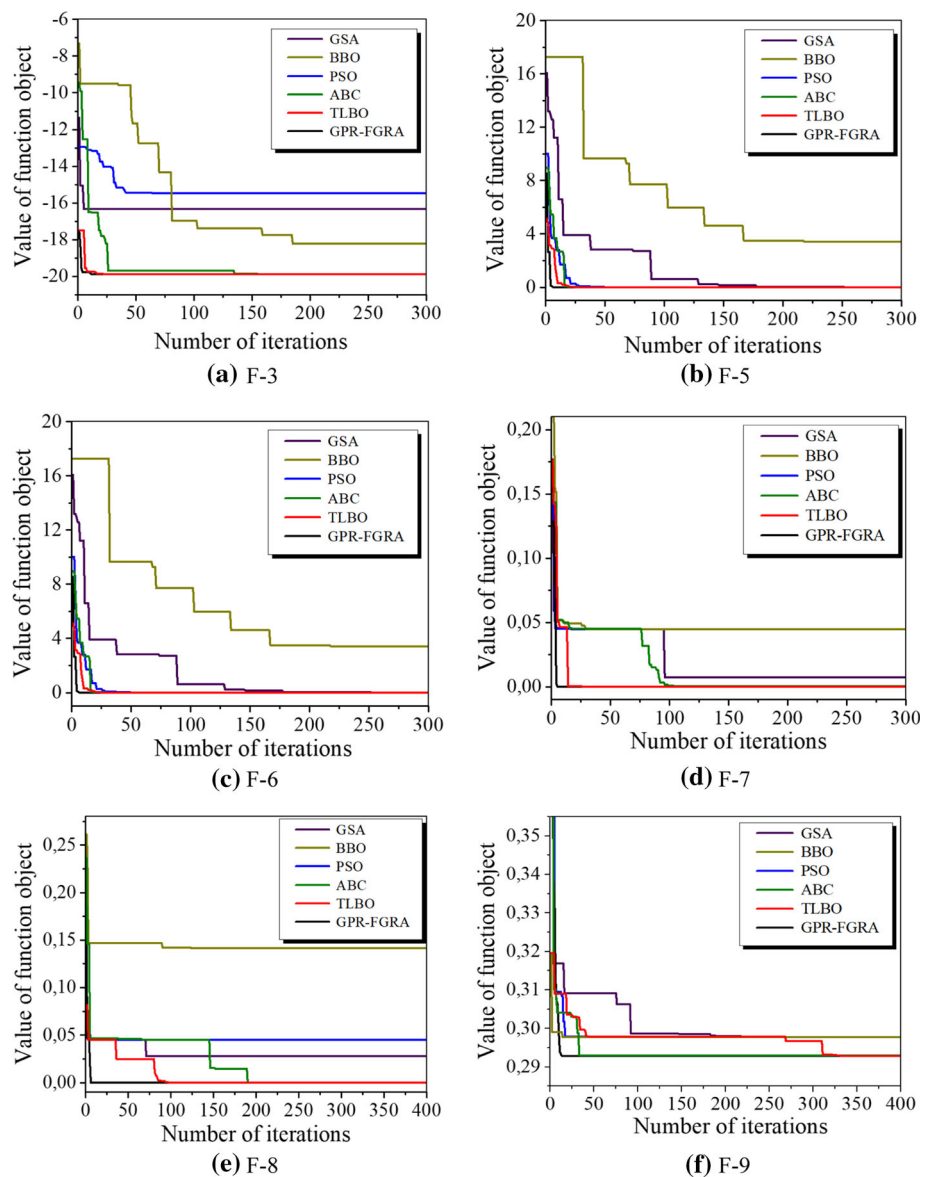


Table 9 Optimal solution with polynomial functions with MRR and surface roughness

Func	Characteristics	Optimization algorithms					
		GSA	BBO	PSO	ABC	TLBO	GPR-FGRA
F-10	Time reached	25.5	31	37.5	40	41.5	24.01
	OA value	16	17.5	18	18.2	18.5	19.1
F-11	Time reached	26	31.5	38.2	41	42.3	24
	OA value	0.038	0.035	0.033	0.031	0.028	0.025

speed and MRF carrier speed. It can find that the MRR values decrease as the working distance (K) increases. As our previous study [28] mentioned, the higher working distance leads to the APs force acting on the surface machining more minor in the MRF process; therefore, MRR will reduce. K = 1 mm at the working distance for the highest material removal rate capacity. When the workpiece speed and the MRF carrier

speed increase. The cutting speed between the APs and the workpiece increases, thereby increasing the ability to remove residual material.

The results obtained in Fig. 11b, c show that the relationship between the feed rate, the MRF carrier speed and the workpiece speed to MRR value is quite complex. Figure 14b illustrates that the workpiece speed in the range of 1000–1200

Fig. 7 MRR prediction under different polishing experiments conditions

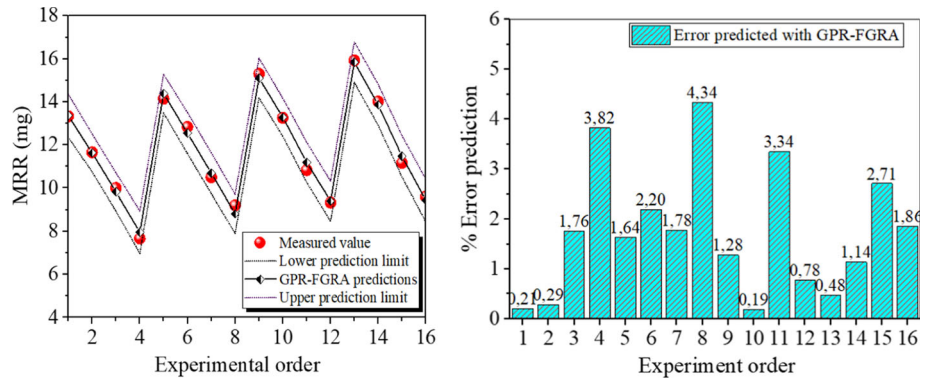


Fig. 8 Predictive results of surface quality under different polishing conditions

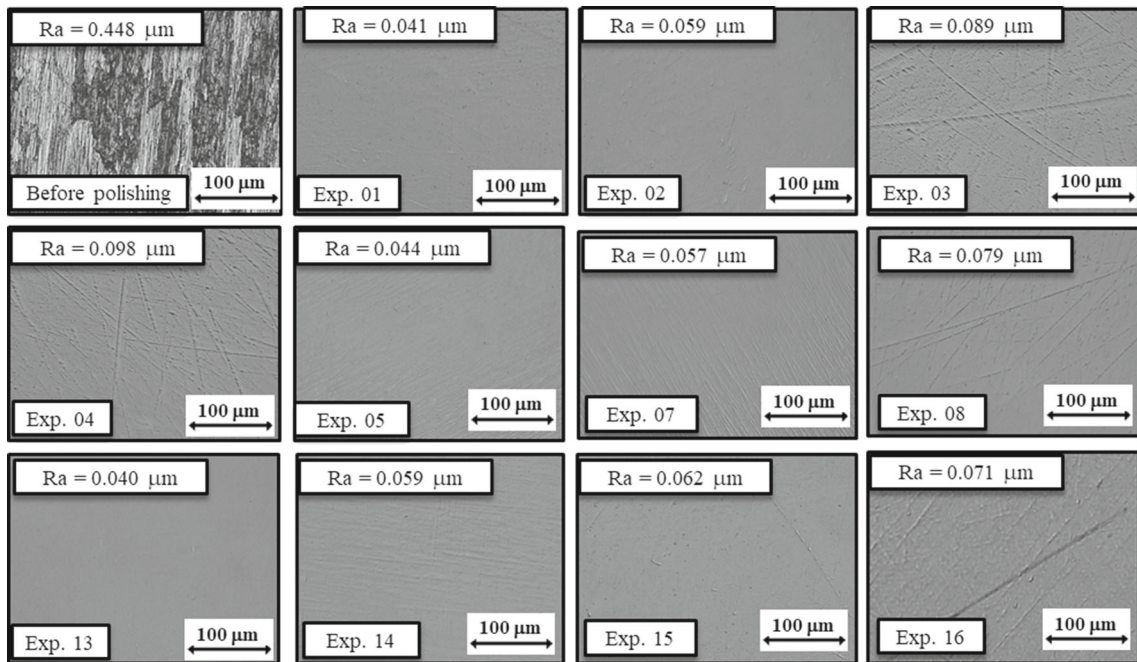
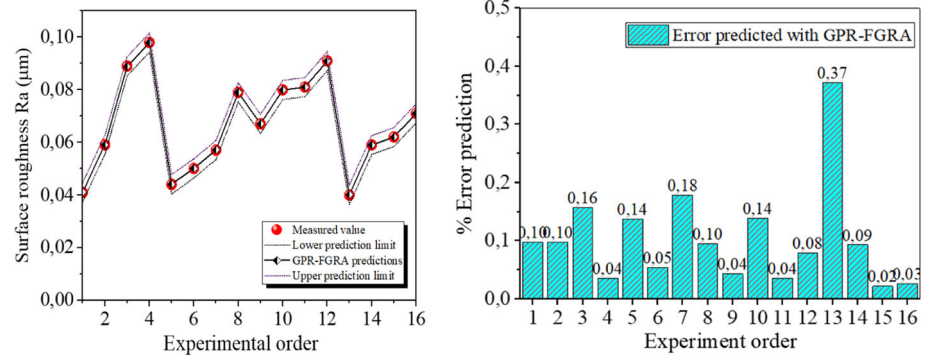


Fig. 9 Surface roughness and morphology after MRF polishing of Ti-6Al-4V alloy under different experimental conditions

(rpm) and the MRF carrier speed of 25–30 rpm gives a small MRR value. With the workpiece speed in the range of 1000–1200 (rpm) and the MRF carrier speed increased to 35–40 rpm, the MRR value increases rapidly. Figure 11d shows the influence of workpiece speed and feed rate on the

MRR when the workpiece speed is in the range of 800–1000 (rpm) with a feed of 300–500 (mm/min) for small MRR values, whereas increasing the feed rate between 300 and 500 (mm/min) for high MRR. The relationship between workpiece speed, feed rate and MRF carrier speed to MRR is

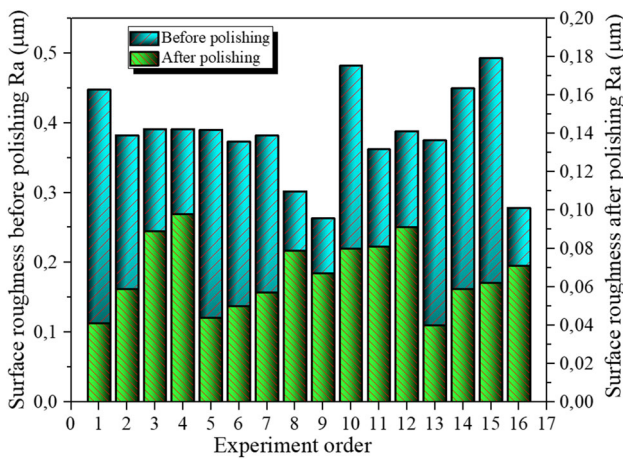


Fig. 10 Surface roughness of workpiece before and after 90 min of polishing under different test conditions

complex. Still, it seems that a high MRR value corresponds to a significant workpiece speed, feed rate and MRF carrier speed. With these factors increased, the relative cutting speed between the APs and the workpiece increases, thereby improving the ability to remove excess workpiece material.

The analysis results in Fig. 12 show that the relationship between technological parameters and surface quality is quite complicated. However, it can be seen that the slight surface roughness corresponding to the range of the working distance, workpiece speed, feed rate and MRF carrier speed is 1–1.2 mm, 500–600 rpm, 25–30 (mm/min) and 25–35 rpm, respectively. The analysis results show that when the working distance is low ($K = 1-1.2$ mm), the impact force of the APs on the workpiece increases, thereby giving an excellent ability to remove the workpiece material leading to surface roughness decreases. In comparison, the high rotation of the MRF carrier will cause uneven material removal as the abrasive particles to move away from the centre due to centrifugal force in the MRF process. Therefore, the surface quality degrades with higher MRF carrier speed.

To determine the influence of technological factors such as workpiece speed, polishing distance, MRF carrier speed and feed rate to Ra and MRR. The factors affecting MRR and Ra are determined through the GPR-FGRA coefficient with comparison and reference matrix as described below:

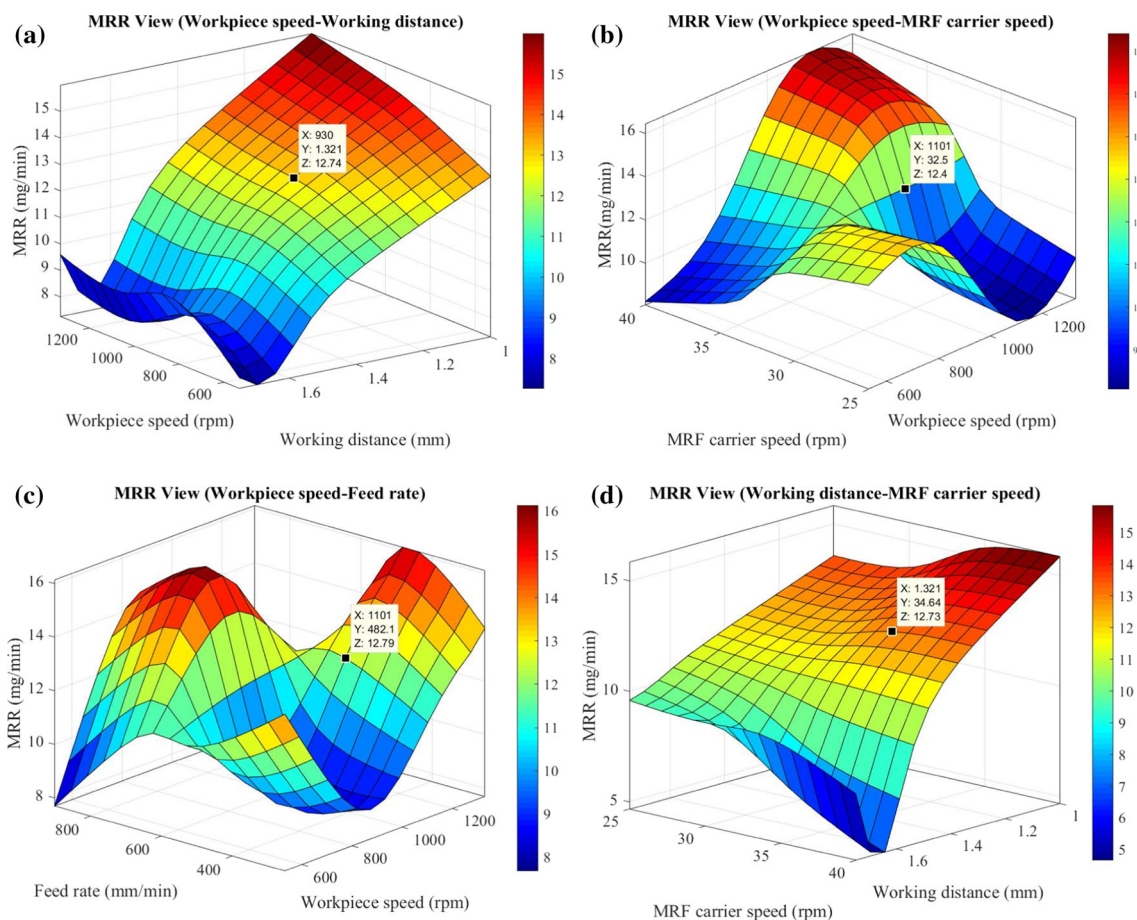


Fig. 11 Effect of workpiece speed, working distance, MRF carrier and F to MRR

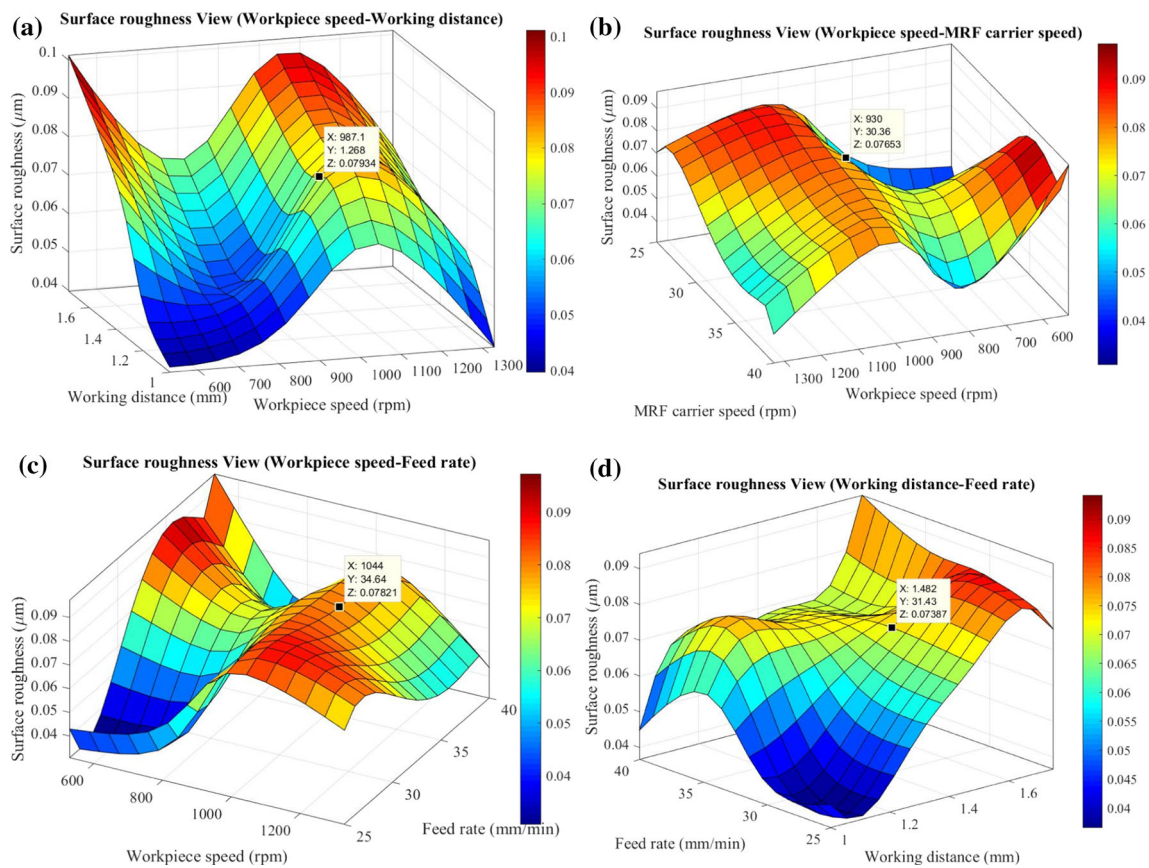


Fig. 12 Effect of workpiece speed, working distance, MRF carrier and F to Ra

$$\begin{matrix} Y_1(x) \\ Y_2(x) \\ Y_3(x) \\ Y_4(x) \\ Y(x) \end{matrix} = \begin{bmatrix} 530 & 530 & 530 & 530 & 720 & 720 & 720 & 720 & 980 & 980 & 980 & 980 & 1330 & 1330 & 1330 & 1330 \\ 1 & 1, 25 & 1, 50 & 1, 75 & 1 & 1, 25 & 1, 50 & 1, 75 & 1 & 1, 25 & 1, 50 & 1, 75 & 1 & 1, 25 & 1, 50 & 1, 75 \\ 25 & 30 & 35 & 40 & 30 & 25 & 40 & 35 & 35 & 40 & 25 & 30 & 40 & 35 & 30 & 25 \\ 250 & 500 & 750 & 900 & 750 & 900 & 250 & 500 & 750 & 900 & 500 & 250 & 500 & 250 & 900 & 750 \\ 13, 33 & 11, 66 & 10 & 7, 67 & 14, 15 & 12, 83 & 10, 50 & 9, 21 & 15, 30 & 13, 26 & 10, 83 & 9, 33 & 15, 92 & 14, 02 & 11, 17 & 9, 60 \end{bmatrix} \quad (8)$$

$$\begin{matrix} Z_1(x) \\ Z_2(x) \\ Z_3(x) \\ Z_4(x) \\ Z(x) \end{matrix} = \begin{bmatrix} 530 & 530 & 530 & 530 & 720 & 720 & 720 & 720 & 980 & 980 & 980 & 980 & 1330 & 1330 & 1330 & 1330 \\ 1 & 1, 25 & 1, 50 & 1, 75 & 1 & 1, 25 & 1, 50 & 1, 75 & 1 & 1, 25 & 1, 50 & 1, 75 & 1 & 1, 25 & 1, 50 & 1, 75 \\ 25 & 30 & 35 & 40 & 30 & 25 & 40 & 35 & 35 & 40 & 25 & 30 & 40 & 35 & 30 & 25 \\ 250 & 500 & 750 & 900 & 750 & 900 & 250 & 500 & 750 & 900 & 500 & 250 & 500 & 250 & 900 & 750 \\ 0, 041 & 0, 059 & 0, 089 & 0, 098 & 0, 044 & 0, 050 & 0, 057 & 0, 079 & 0, 067 & 0, 080 & 0, 081 & 0, 091 & 0, 040 & 0, 059 & 0, 062 & 0, 071 \end{bmatrix} \quad (9)$$

Figures 9 and 10 illustrate four factors of fuzzy membership classes that affect polishability through the output parameters Ra and MRR. The fuzzy member layer results analysis showed that with MRR, the highest index corresponds to the workpiece speed (0.7654), then MRF carrier speed (0.7148) and feed rate (0.6982). Meanwhile, the working distance has the lowest value (0.6185). There is a significant difference in the analytical results between MRR

and Ra. At the lowest level is the workpiece speed change (0.5921), followed by MRF carrier speed (0.7383) and the feed rate (0.7487), with the shift of polishing distance K valid the largest (0.7805). Thus surface quality will be affected by polishing distance (K) being the largest and the workpiece speed being the smallest. Whereas MRR tends opposite to Ra, the workpiece speed has the most significant effect, while the working distance K has the slightest influence on MRR.

Fig. 13 The results analysis of the fuzzy grey relationship with MRR

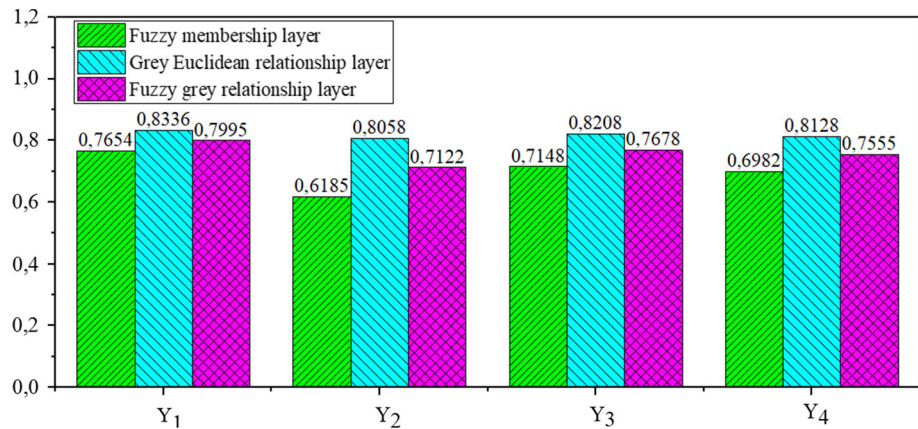
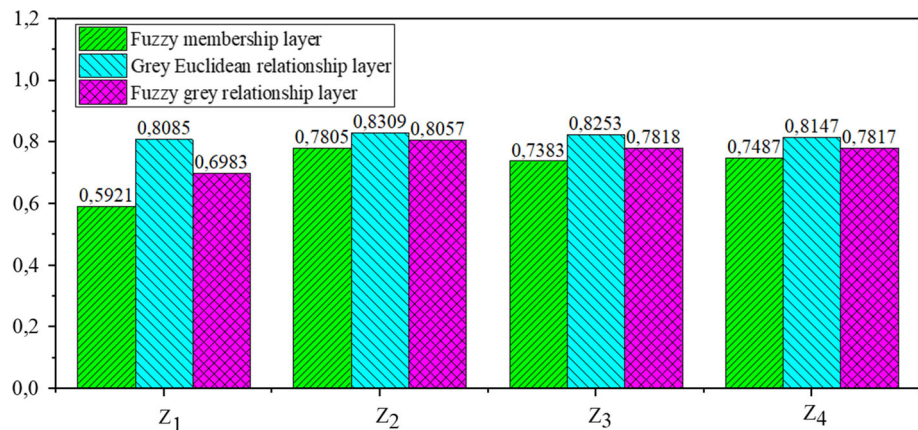


Fig. 14 The results analysis of the fuzzy grey relationship with Ra



As shown in Figs. 13 and 14, the grey Euclidean relation layer of the four elements in the polishing process, show negligible differences. However, it still shows that with MRR, the grey Euclidean relation layer of the workpiece speed is highest. The grey Euclidean relation layer of the working distance (K) is the highest with Ra. Therefore, when it is necessary to improve the surface quality, we should focus on changing the working distance (K), then the MRF carrier speed and feed rate. Meanwhile, changing workpiece speed has the most influence on MRR compared to changing the remaining parameters.

The fuzzy grey relationship layer of the four factors up to the surface polishability, as shown in Figs. 13 and 14. The analysis provides an overview to evaluate survey factors that affect the MRR and Ra. The fuzzy grey relationship layer for the Ra of the four elements (workpiece speed, working distance, MRF carrier speed and feed rate) corresponds to 0.6983, 0.8057, 0.7818, and 0.7817. Whereas with MRR, the fuzzy grey relationship layer to technological parameters is shown by 0.7995, 0.7122, 0.7678 and 0.7555. Therefore, when MRF polishes Ti–6Al–4V alloy, the working distance must first be chosen when super smooth surface quality is required. Workpiece speed is the priority when increasing productivity and reducing polishing time.

According to the GPR-FGRA algorithm, the proposed optimization model gives the optimal parameters for the best surface quality. The results of different optimization models as described in Table 10. The surface quality obtained with the GPR-FGRA proposed algorithm is significantly improved ($Ra = 0.025$ mm) compared with the Taguchi experimental method ($Ra = 0.040$ mm). Thus, the surface quality increased by 37.5% when choosing the optimized cutting parameter with the GPR-FGRA hybrid algorithm.

5 Conclusions

This study introduced a new polishing method with MRF containing inexpensive CIPs and APs. The carrier liquid is a safe and eco-friendly cutting oil solution combined with a new GPR-FGRA hybrid algorithm for an ultra-precise mirror polishing surface Ti–6Al–4V alloy. According to work done, the main conclusions as description follows:

- Introduced ultra-precise machining models for expensive, difficult-to-machine materials from highly commercial

Table 10 The best experimental and optimized cutting parameter results

Optimize surface quality	n_w (rpm)	K (mm)	n_{MRF} (rpm)	F (mm/min)	Ra (μm)
Best cutting parameters by Taguchi experiment	1330	1	40	500	0.040
Optimal cutting parameters by GPR-FGRA	1350.28	1.15	28.18	404.85	0.025

and environmentally friendly materials. The polishing carrier liquid is established based on miscible oil cutting fluid of natural origin, low-cost CIPs and APs.

- A new GPR-FGRA hybrid algorithm proposes for predicting and optimizing MRF polishing of Ti–6Al–4V alloy. From analytical results with the proposed algorithm, the quality obtained by GPR-FGRA is superior to the algorithms mentioned in most cases. Thereby shows the high applicability of GPR-FGRA for the polishing problem and application to other prediction and optimization objects.
- The polishing Ti–6Al–4V material yielded the fuzzy grey relationship layer for the Ra of the four elements (workpiece speed, working distance, MRF carrier speed and feed rate) corresponding to 0.6983, 0.8057, 0.7818, and 0.7817. Whereas with MRR, the fuzzy grey relationship layer to technological parameters is shown by 0.7995, 0.7122, 0.7678 and 0.7555. Therefore, when MRF polishes Ti–6Al–4V alloy, the working distance must first be chosen when super smooth surface quality is required; workpiece speed is the priority when increasing productivity and reducing polishing time.
- The analysis results with the proposed MRF polishing model get out superfine Ti–6Al–4V alloy surface can be produced with the surface roughness $Ra = 0.025 \mu\text{m}$ according to the parameters $K = 1.15 \text{ mm}$, $n_w = 1350.28 \text{ rpm}$, $n_{MRF} = 28.18 \text{ rpm}$ and $F = 404.85 \text{ mm/min}$. The optimization surface quality increased by 37.5% and gave the prediction accuracy greater than 99.63% when choosing the optimized and prediction with the GPR-FGRA hybrid algorithm, respectively. Hence the polishing process using MRF and the proposed algorithm with inexpensive CIP and AP particles and vegetable oil carrier liquid has excellent potential to create an ultra-fine Ti–6Al–4V surface without affecting the environment and high efficiency.

Declarations

Conflict of interest The authors have nothing to disclose and no conflict of interests regarding the publication of this paper.

References

1. Yin, S., Nguyen, D., Chen, F., Tang, Q., Duc, L.A.: Application of compressed air in the online monitoring of surface roughness and grinding wheel wear when grinding Ti–6Al–4V titanium alloy. *Int. J. Adv. Manuf. Technol.* **101**, 1315–1331 (2018)
2. Nguyen, D., Yin, S., Tang, Q., Son, P.X., Duc, L.A.: Online monitoring of surface roughness and grinding wheel wear when grinding Ti–6Al–4V titanium alloy using ANFIS-GPR hybrid algorithm and Taguchi analysis. *Precis. Eng.* **55**, 275–292 (2019)
3. Ju, J., Li, J., Yang, C., Wang, K., Kang, M., Wang, J.: Evolution of the microstructure and optimization of the tensile properties of the Ti–6Al–4V alloy by selective laser melting and heat treatment. *Mater. Sci. Eng. A* **802**, 140673 (2021)
4. Tümer, D., Güngörürler, M., Havitçioğlu, H., Arman, Y.: Investigation of effective coating of the Ti–6Al–4V alloy and 316L stainless steel with graphene or carbon nanotubes with finite element methods. *J. Mater. Res. Technol.* **9**, 15880–15893 (2020)
5. Siva Surya, M., Gugulothu, S., Prasanthi, G.: Optimization of cutting parameters while turning Ti–6Al–4V using response surface methodology and machine learning technique. *Int. J. Interact. Des. Manuf. (IJIDeM)* **15**, 453–462 (2021)
6. Qian, N., Fu, Y., Chen, J., Khan, A.M., Xu, J.: Axial rotating heat-pipe grinding wheel for eco-benign machining: a novel method for dry profile-grinding of Ti–6Al–4V alloy. *J. Manuf. Process.* **56**, 216–227 (2020)
7. Zhao, B., Jiang, G., Ding, W., Xiao, G., Huan, H., Wang, Y., et al.: Characterisation of the wear properties of a single-aggregated cubic boron nitride grain during Ti–6Al–4V alloy grinding. *Wear* **452–453**, 203296 (2020)
8. Siva Surya, M.: Optimization of turning parameters while turning Ti–6Al–4V titanium alloy for surface roughness and material removal rate using response surface methodology. *Mater. Today Proc.* **62**, 3479–3484 (2022)
9. Luo, H., Yin, S., Zhang, G., Liu, C., Tang, Q., Guo, M.: Optimized pre-thinning procedures of ion-beam thinning for TEM sample preparation by magnetorheological polishing. *Ultramicroscopy* **181**, 165–172 (2017)
10. Duy Trinh, N., Nhat Tan, N., Quang, N.M., Thi Thieu Thoa, P., Duc, L.A.: Application of magnetic liquid slurries and fuzzy grey analysis in polishing nickel-phosphorus coated SKD11 steel. *Particul. Sci. Technol.* **40**, 401–414 (2021)
11. Kumar, S., Jain, V.K., Sidpara, A.: Nanofinishing of freeform surfaces (knee joint implant) by rotational-magnetorheological abrasive flow finishing (R-MRAFF) process. *Precis. Eng.* **42**, 165–178 (2015)
12. Das, M., Barman, A.: Force analysis during spot finishing of titanium alloy using novel tool in magnetic field assisted finishing process. *Int. J. Precis. Technol.* **8**, 190 (2019)
13. Barman, A., Das, M.: Toolpath generation and finishing of bio-titanium alloy using novel polishing tool in MFAF process. *Int. J. Adv. Manuf. Technol.* **100**, 1123–1135 (2019)

14. Nagdeve, L., Jain, V.K., Ramkumar, J.: Preliminary investigations into nano-finishing of freeform surface (femoral) using inverse replica fixture. *Int. J. Adv. Manuf. Technol.* **100**, 1081–1092 (2019)
15. Barman, A., Das, M.: Magnetic field assisted finishing process for super-finished Ti alloy implant and its 3D surface characterization. *J. Micromanuf.* **1**, 251659841878550 (2018)
16. Singh, H., Prakash, C., Singh, S.: Plasma spray deposition of HA-TiO₂ on β -phase Ti–35Nb–7Ta–5Zr alloy for hip stem: characterization of bio-mechanical properties, wettability, and wear resistance. *J. Bionic Eng.* **17**, 1029–1044 (2020)
17. Rao, P.S., Jain, P.K., Dwivedi, D.K.: Optimization of key process parameters on electro chemical honing (ECH) of external cylindrical surfaces of titanium alloy Ti 6Al 4V. *Mater. Today Proc.* **4**, 2279–2289 (2017)
18. Kong, D., Chen, Y., Li, N.: Gaussian process regression for tool wear prediction. *Mech. Syst. Signal Process.* **104**, 556–574 (2018)
19. Zhang, J., Wang, T., Xu, L., Wang, P., Zhang, M., Xu, M.: Development and validation of a prognostic model based on the albumin-to-fibrinogen ratio (AFR) and gamma-glutamyl transpeptidase-to-platelet ratio (GPR) in hepatocellular carcinoma patients. *Clin. Chim. Acta* **511**, 107–116 (2020)
20. Olabanji, O.M., Mpofu, K.: Appraisal of conceptual designs: coalescing fuzzy analytic hierarchy process (F-AHP) and fuzzy grey relational analysis (F-GRA). *Results Eng.* **9**, 100194 (2021)
21. Zeng, J.E.Y., Jin, Y., Zhang, B., Huang, Z., Wei, K., et al.: Heat dissipation investigation of the power lithium-ion battery module based on orthogonal experiment design and fuzzy grey relation analysis. *Energy* **211**, 118596 (2020)
22. Roobahani, A., Ghased, H., Hashemy Shahedany, M.: Inter-basin water transfer planning with grey COPRAS and fuzzy COPRAS techniques: a case study in Iranian Central Plateau. *Sci. Total Environ.* **726**, 138499 (2020)
23. Siva Surya, M., Vepa, K.S., Karanam, M.: Optimization of machining parameters using ANOVA and grey relational analysis while turning aluminium 7075. *Int. J. Recent Technol. Eng.* **8**, 5682–5686 (2019)
24. Hema Latha, K., Usha Sri, P., Seetharamaiah, N.: Design and manufacturing aspects of magneto-rheological fluid (MRF) clutch. *Mater. Today Proc.* **4**, 1525–1534 (2017)
25. Shahinian, H., Cherukuri, H., Mullany, B.: Evaluation of fiber-based tools for glass polishing using experimental and computational approaches. *Appl. Opt.* **55**, 4307–4316 (2016)
26. Fengdong, Z., Xuejun, Z., Jingchi, Y.: Mathematics model of magnetorheological finishing. In: *Proceedings of the SPIE* (2000)
27. Pal, A., Chatha, S.S., Sidhu, H.S.: Experimental investigation on the performance of MQL drilling of AISI 321 stainless steel using nano-graphene enhanced vegetable-oil-based cutting fluid. *Tribol. Int.* **151**, 106508 (2020)
28. Nguyen, D., Wu, J., Quang, N.M., Duc, L.A., Son, P.X.: Applying fuzzy grey relationship analysis and Taguchi method in polishing surfaces of magnetic materials by using magnetorheological fluid. *Int. J. Adv. Manuf. Technol.* **112**, 1675–1689 (2021)
29. Duc, L.A., Li, K., Nguyen, T.T., Yen, V.M., Truong, T.K.: A new effective operator for the hybrid algorithm for solving global optimisation problems. *Int. J. Syst. Sci.* **49**, 1088–1102 (2018)
30. Parameswari, G., Jain, V.K., Ramkumar, J., Nagdeve, L.: Experimental investigations into nanofinishing of Ti6Al4V flat disc using magnetorheological finishing process. *Int. J. Adv. Manuf. Technol.* **100**, 1055–1065 (2019)

Publisher's Note Springer Nature remains neutral with regard to jurisdictional claims in published maps and institutional affiliations.

Springer Nature or its licensor holds exclusive rights to this article under a publishing agreement with the author(s) or other rightsholder(s); author self-archiving of the accepted manuscript version of this article is solely governed by the terms of such publishing agreement and applicable law.